Analysis of the intergrain critical state of polycrystalline $YBa_2Cu_3O_{7-\delta}$ using hollow cylinders

Patrick Fournier and Marcel Aubin
Département de Physique and Centre de Recherche en Physique du Solide, Université de Sherbrooke, Sherbrooke, Québec, Canada J1K 2R1
(Received 23 December 1993)

The magnetic field in the center of a superconducting $YBa_2Cu_3O_{7-\delta}$ hollow cylinder is measured as a function of the applied field for temperatures ranging from 20 to 85 K. The aim of this paper is to explain the low-field hysteresis of the magnetization encountered in this and similar polycrystalline materials through the use of the generalized critical state model. Parameters of the model are determined by fitting the data giving an exponent close to $n=2$, a zero field critical current density J_{c0} ranging from 0 to 1300 A/cm^2, and a characteristic field H_0 which varies from 0 to 125 G. A related study of the full penetration field as a function of the wall thickness is also presented. We include the effect of the demagnetizing factor in the theoretical analysis when the cylinders are short compared to their diameter and their wall thickness. This leads to a shielded volume fraction f_g of the sample of around 0.55.

I. INTRODUCTION

Since the discovery of high-temperature superconductivity,[1] many workers have observed two hysteresis loops in the magnetization curves of the Y-Ba-Cu-O (YBCO) polycrystalline system (see Ref. 2 and references therein). One appears at high applied fields (above, say, 500 G) and is associated with the bulk critical current density J_{cg} induced in the grains, which are then decoupled and penetrated by vortices. At lower applied fields (0–200 G), another loop is observed and corresponds to vortices in the intergrain regions associated with a critical current density J_{cj} flowing in the weak-link network throughout the sample. At intermediate fields, a combination of both effects is expected (this is confirmed by the hysteresis of the transport critical current of such samples[3,4]).

Since the intergrain contribution is intimately related to the critical current limitation[5] and J_{cj} is field dependent,[6] we want to focus on the mechanism of pinning for the corresponding intergrain vortices and its influence on the magnetic properties of YBCO. We choose to study hollow cylinders[7] since it is then possible to obtain a direct solution of the field in the center as a function of the field at the surface of the cylinder from the critical state equation.

Measurements of the magnetic state of superconductors using cylinders were first introduced by Kim, Hampstead, and Strnad[8] on Nb-Sn and Nb-Zr tubes. Using magnetoresistant probes, they obtained the magnetic field in the hole as a function of the applied magnetic field. They related the data to a critical state model following an empirical function for $J_c(H)$ given by $J_c(H)=\alpha(H+H_0)^{-1}$ in which α and H_0 are material- and temperature-dependent parameters. Many authors[7,9–14] have presented hollow cylinder data showing the irreversibility observed at low fields in YBCO. Such data allow a determination of the full penetration field H_p and other characteristic fields as a function of temperature and wall thickness a. In particular, the wall thickness dependence[14] can be a valuable source of information since $H_p(a)$ includes in general all the parameters of a given critical state expression for $J_c(H)$.

To analyze our data, we use the generalized critical state model[15] (GCSM), which unifies the Bean, linear, exponential, and Kim models. It includes three parameters that we obtain by fitting the magnetic field measured in the center of the hollow cylinder H_{cent} as a function of the applied field H_a. In this paper, we first show that these parameters can be determined completely even before fitting the data using the derivative of H_{cent} with respect to H_a at given points of the hysteresis loop for infinitely long hollow cylinders. Because we expect and observe demagnetizing effects with our short cylinders, this technique cannot be used. An additional contribution is included in a theoretical model in which the demagnetizing factor and the shielded volume fraction of the cylinder are introduced. In the case of short cylinders, we underline the fact that the trapped field is not the full penetration field H_p. Nevertheless, we develop a method to extract H_p from the data using $\partial H_{\text{cent}}/\partial H_a$. It is then possible to fit the experimental data and determine the GCSM parameters as a function of temperature.

II. THEORETICAL APPROACH

The GCSM in cylindrical coordinates is given by[15]

$$J_{cj}(r)=\frac{dH(r)}{dr}=\frac{\pm J_{c0}}{(1+|H(r)|/H_0)^n}\ , \tag{1}$$

where J_{c0}, H_0, and n are the parameters related to the intergrain coupling and to the pinning type and strength. These parameters are expected to be temperature dependent. The sign of J_{cj} is determined by the local variation of the intergrain field $H(r)$ as the applied field varies (+: $|H(r)|$ increases; −: $|H(r)|$ decreases). A schematic of the cylinder and its corresponding field profiles

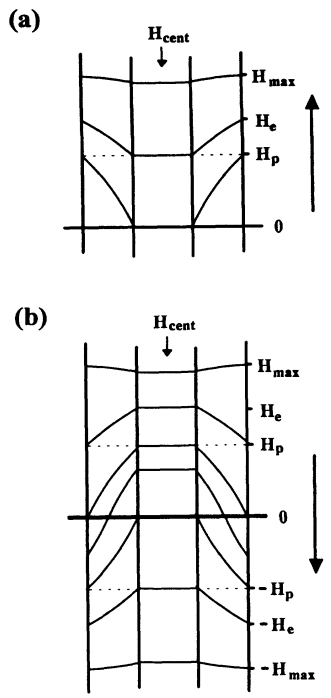

FIG. 1. Flux profiles obtained while sweeping the magnetic field from (a) 0 to H_{max}, (b) H_{max} to $-H_{max}$.

is presented in Fig. 1. In the following subsection, we suppose that $H(r)$ never exceeds the lower critical field of the grains (H_{c1g}) and that weak-link lower critical field H_{c1w} is negligible.[16]

A. Infinitely long hollow cylinders

Solving for the field in the center of an infinitely long hollow cylinder (zero demagnetizing factor) of wall thickness a as a function of the effective field at the surface H_{eff} gives

$$H_{cent}=[(|H_{eff}|+H_0)^{n+1} \mp(n+1)J_{c0}H_0^n a]^{1/(n+1)}-H_0 , \quad (2)$$

where $-$ and $+$ are for the ascending and descending branches, respectively. We are also able to determine the full penetration field H_p and the field H_e at which $H_{cent}=H_p$ on the ascending branch (see Fig. 1):

$$H_p=H_0\{[1+(n+1)J_{c0}a/H_0]^{1/(n+1)}-1\} \quad (3)$$

and

$$H_e=H_0\{[1+2(n+1)J_{c0}a/H_0]^{1/(n+1)}-1\} . \quad (4)$$

We see that these characteristic fields depend on the same three parameters (J_{c0}, H_0, and n) and that the trapped field is given by H_p [see Fig. 1(b) when $H_{eff}=0$]. It will be seen that an accurate fit of $H_p(a)$ remains difficult in YBCO since low wall thicknesses (below 1 mm) become necessary. However, a direct determination of J_{c0}, H_0, and n can be obtained if we use the derivative of $H_{cent}(H_{eff})$ at various points of the hysteresis loop.

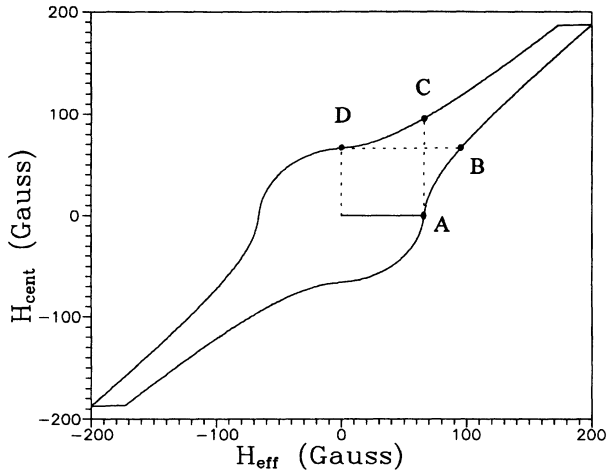

FIG. 2. Theoretical H_{cent} as a function of H_{eff} for $J_{c0}=1000$ A/cm^2, $H_0=5$ G, $n=1$, and $a=4$ mm.

In Fig. 2 we illustrate the theoretical loop for an arbitrary but realistic set of J_{c0}, H_0, and n values. Using Eq. (2), the derivative of H_{cent} gives

$$\frac{\partial H_{cent}}{\partial H_{eff}}=\left[1\mp\frac{(n+1)J_{c0}H_0^n a}{(|H_{eff}|+H_0)^{n+1}}\right]^{-n/(n+1)} , \quad (5)$$

with $-$ and $+$ for the ascending and descending branches, respectively. At point B ($H_{eff}=H_e$, ascending branch) this gives

$$\frac{\partial H_{cent}}{\partial H_{eff}}=\left[\frac{H_e+H_0}{H_p+H_0}\right]^n\equiv\beta \quad (6)$$

and, at point D ($H_{eff}=0$, descending branch),

$$\frac{\partial H_{cent}}{\partial H_{eff}}=\left[\frac{H_0}{H_p+H_0}\right]^n\equiv\gamma , \quad (7)$$

where Eqs. (3) and (4) have been used. Since β, γ, H_p, and H_e can be obtained experimentally, we are able to uniquely determine n and H_0 (and eventually J_{c0} with the expression for H_p). In fact, one can prove that n is the solution of

$$\frac{H_p}{H_e}=\frac{1-\gamma^{1/n}}{\beta^{1/n}-\gamma^{1/n}} , \quad (8)$$

which helps us to find H_0:

$$H_0=\frac{\gamma^{1/n}H_p}{1-\gamma^{1/n}} . \quad (9)$$

J_{c0} may be obtained directly from Eq. (3):

$$J_{c0}=\frac{H_0}{(n+1)a}\left\{\left[\frac{H_p}{H_0}+1\right]^{n+1}-1\right\} . \quad (10)$$

In principle, these three basic equations should be sufficient to determine the parameters of the GCSM.

B. Demagnetizing effect for short cylinders

Another important contribution influences the experimental data. This is the demagnetizing or shape effect. For very long hollow cylinders, the demagnetizing factor N is zero and there is no difference between the applied magnetic field H_a and the surface or effective field H_{eff}. This will not be the case with our data, which show a demagnetizing effect. For this reason, Eqs. (8) and (9) cannot be used because β and γ are influenced by this effect. These equations are only valid when one measures H_{cent} of sufficiently long hollow cylinders (typically with the same aspect ratios as those of the original Kim-Hampstead-Strnad[8] work).

Thus we use a simplified version of several works on the calculation of the low-field magnetization[16–18] of these materials in which we suppose that the grains are long filaments of zero demagnetizing factor. Furthermore, our calculations will be restricted to cases in which the grains remain in the Meissner state [we suppose $H(r)$ smaller than H_{c1g} everywhere in the sample]. When the cylinders are short enough to obtain aspect ratios (diameter/length or wall thickness/length) of the order of 1, the effective field H_{eff} at the sample surface with a demagnetizing factor N is

$$H_{\text{eff}}=H_a-NM \ , \tag{11}$$

where M is the total magnetization of the sample at H_{eff} (or the corresponding H_a). To simulate the demagnetizing effects, one has to obtain $M(H_{\text{eff}})$ and inject this value in Eq. (11): This gives a relation between H_{eff} and H_a for given values of N and wall thickness a.

The magnetization contains two contributions: One is related to the screening intergrain current density and the other to the individual screening of each grain. The latter one, M_g, can be written as

$$M_g=\frac{f_g}{V}\int_V d^3r\,\chi_g H(r) \ , \tag{12}$$

where $H(r)$ is the intergrain field (solution of the GCSM), $\chi_g(=-1)$ is the susceptibility of the grains below H_{c1g}, V is the total volume of the sample, and f_g is the shielded volume fraction of the sample. Here we have supposed that f_g is a constant throughout the sample, which is true if the grains all have the same radius. Since we expect a distribution of grain radii to occur, Eq. (12) is only a rough approximation. We can rewrite Eq. (12) as

$$M_g=\chi_g f_g\langle H(r)\rangle_{\text{inter}} \ , \tag{13}$$

where $\langle H(r)\rangle_{\text{inter}}$ is the mean field in the sample. One can see that it is an irreversible contribution since $\langle H(r)\rangle_{\text{inter}}$ is different for ascending and descending branches (for the same H_{eff}). The other contribution comes from the macroscopic intergrain current density J_{cj}, which gives a magnetization

$$M_{\text{inter}}=\langle H(r)\rangle_{\text{inter}}-H_{\text{eff}} \ . \tag{14}$$

Thus the total magnetization is given by

$$M(H_{\text{eff}})=(1+\chi_g f_g)\langle H(r)\rangle_{\text{inter}}-H_{\text{eff}} \ . \tag{15}$$

Using Eqs. (11) and (15), we finally obtain for H_a as a function of H_{eff}:

$$H_a=(1-N)H_{\text{eff}}+N(1+\chi_g f_g)\langle H(r)\rangle_{\text{inter}} \ . \tag{16}$$

To obtain H_a, one has to calculate $\langle H(r)\rangle_{\text{inter}}$, which can be obtained analytically (see the Appendix). We have to underline the fact that for high enough applied fields $H(r)$ becomes constant throughout the sample as shown in Fig. 1(a) for $H_{\text{eff}}=H_{\max}$ (when J_{cj} is a decreasing function of H). This results in $H_{\text{cent}}\to H_{\text{eff}}$ and $\langle H(r)\rangle_{\text{inter}}\to H_{\text{eff}}$, giving

$$H_a\to(1+N\chi_g f_g)H_{\text{eff}} \ . \tag{17}$$

This implies that the experimental $\partial H_{\text{cent}}/\partial H_a$ should tend to a constant $[1/(1-Nf_g)]$ which determines uniquely the product Nf_g.

In Fig. 3 we show the effect of the demagnetizing factor on the calculated H_{cent} as a function of H_a for given values of N, f_g, J_{c0}, H_0, n, and a. The presence of a demagnetizing factor (and of f_g) increases the mean slope of the loop. We also note the slight effect of various N and f_g values, keeping the product Nf_g constant. It seems that the trapped field is not really influenced by this variation. However, the applied field $H_p'=H_p+NM(H_p)$ at which $H_{\text{cent}}=0$ shifts as N and f_g are modified.

To show that the calculated magnetization has the correct behavior, we made the calculation for a filled cylinder of 3 mm diameter (the wall thickness equals the radius), $J_{c0}=500$ A/cm^2, $H_0=10$ G, $n=1$, $N=0.2$, and $f_g=0.7$. The result is presented in Fig. 4 and agrees qualitatively with the experimental results presented by Senoussi, Oussena, and Hadjoudj[19] at 60 K. One also notes that the width of the loop is principally determined by the factor f_g, while the mean slope is still determined by the Nf_g product.

All this theoretical work clarifies what has to be done

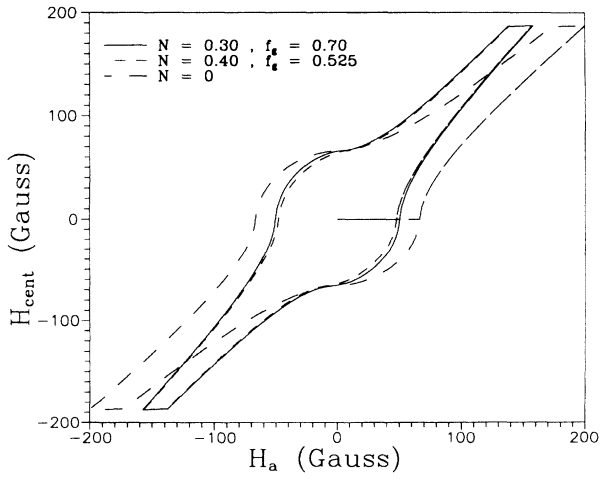

FIG. 3. Theoretical H_{cent} as a function of H_a with $J_{c0}=1000$ A/cm^2, $H_0=5$ G, $n=1$, and $a=4$ mm. The N and f_g values are indicated on the curves.

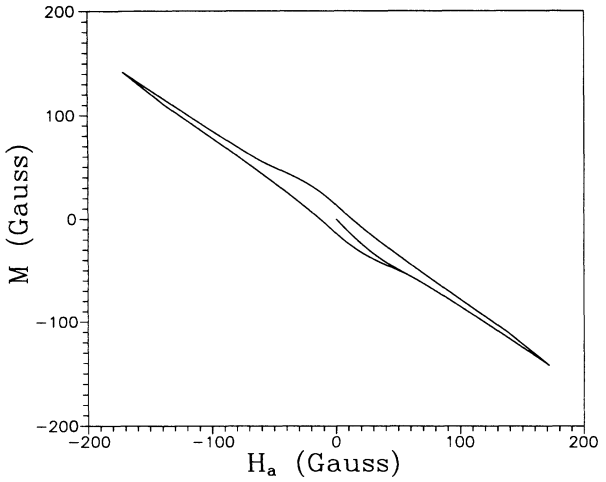

FIG. 4. Example of a magnetization calculation for a closed cylinder with $R=a=3$ mm, $J_{c0}=1000$ A/cm^2, $H_0=10$ G, $n=1$, $f_g=0.70$, and $N=0.2$.

experimentally to determine the GCSM parameters. The obvious choice is to avoid short cylinders or to obtain short cylinders with negligible demagnetizing factors. The latter is achievable if one reduces the wall thickness a. In fact, a thin wall tube can be seen as a closed thin slab (a thin slab has a demagnetizing factor approaching zero). In the following sections we describe measurements of $H_{\rm cent}$ as a function of H_a for different wall thicknesses of YBCO hollow cylinders. We show that the results with the greatest wall thicknesses are easy to fit despite the nonzero N. This allows a determination of J_{c0}, H_0, and n. We verify the validity of these parameters by fitting the wall thickness dependence of the full penetration field H_p. Because of end effects, the theoretical procedure presented above [see Eqs. (8)–(10)] cannot be used to fit accurately the data with small wall thicknesses ($N\rightarrow 0$).

III. EXPERIMENTAL PROCEDURES

Details of the sample preparation are presented elsewhere.[7] The cylinders are obtained by stacking several pellets of approximately 1.5 mm thickness and 12.5 mm outer diameter. All the results presented here are obtained with a cylinder 9 mm in length. A small hole is drilled initially in each pellet and then gradually enlarged by sandblasting, which creates less heat and damage than drilling. This increases the range of available wall thicknesses as the pellets are more and more fragile with increasing hole diameter and ensures that the sample quality is not modified during the whole experiment.

The magnetic field in the hole is measured using an n-type GaAs film ($n=10^{16}$/cm^3) calibrated at various temperatures in the range 20–85 K. The Hall voltage is measured by a Keithley 182 sensitive nanovoltmeter as the current in the probe is fixed at 0.5 mA. This gives an accuracy of the measured field which is better than 0.1 G (largely sufficient compared to the typical $H_{\rm cent}$ of several tens of gauss). All the measurements are made with the sample cooled in zero field (earth field) by a closed-cycle refrigerator giving access to temperatures as low as 10 K. The applied field (and the effective one) never exceeds the lower critical field of the grains (H_{c1g}). If it did exceed H_{c1g}, a decrease of the trapped field would be observed along with additional contributions to the hysteresis loop from intragrain effects.

IV. RESULTS AND DISCUSSION

Figure 5 shows the results obtained with a cylinder of length $L=9$ mm and wall thickness $a=3$ mm at several temperatures. We observe an increase of the trapped field ($H_{\rm cent}$ at $H_a=0$) as the temperature decreases. This reflects the increase of the pinning force with decreasing temperatures. On the other hand, we do not observe a reversible regime at the higher fields in our data. This indicates that we never reach H_{c2j} (the upper critical field of the junction network). Should the magnetic field reach this value, the model would require modifications to fit the results. It is anticipated that H_{c1} is even larger[20] than H_{c2j} as in $La_{1.8}Ba_{0.2}CuO_4$.

The mean slope of the loops remains the same for all temperatures (in the case of Fig. 5, it is $H_{\rm cent}=1.25H_a$). This fixes the product Nf_g in Eq. (17) and shows that it is essentially temperature independent. Equation (17) predicts that, as N varies, the mean slope of the loop is affected: An example of this effect is shown in Fig. 6. As the wall thickness decreases, the factor $1/(1-Nf_g)$ decreases as expected. In the same figure, we observe a significant variation of the trapped field $H_{\rm trapped}$ with the wall thickness. This is expected since for an infinitely long tube, $H_{\rm cent}(H_a=0)=H_p$, which is known to be a function of a [see Eq. (2)]. However, in a real case such as ours for $H_a=0$, the effective field at the surface of the cylinder is $H_{\rm eff}=-NM(H_a=0)$. Since $M(H_a=0)$ is nonzero,[2] the trapped field measured at $H_a=0$ is *not* H_p. To find H_p, one has to use the derivative of $H_{\rm cent}$ with respect to H_a. This gives

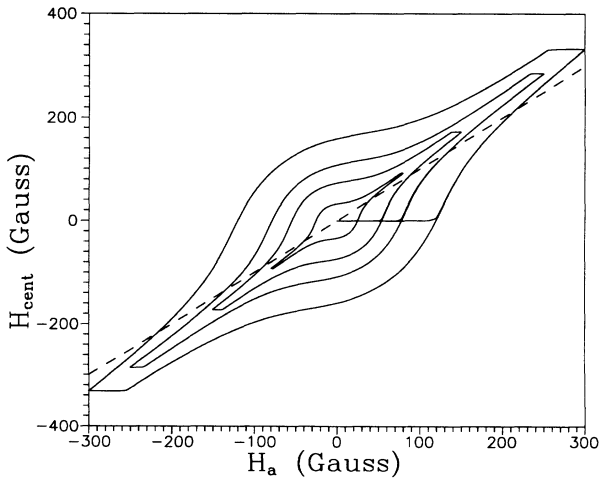

FIG. 5. Experimental $H_{\rm cent}$ as a function of H_a at various temperatures for $a=3$ mm. From the inner to the outer loop: 80, 65, 50, and 20 K. Also shown $H_{\rm cent}=H_a$ (dashed line).

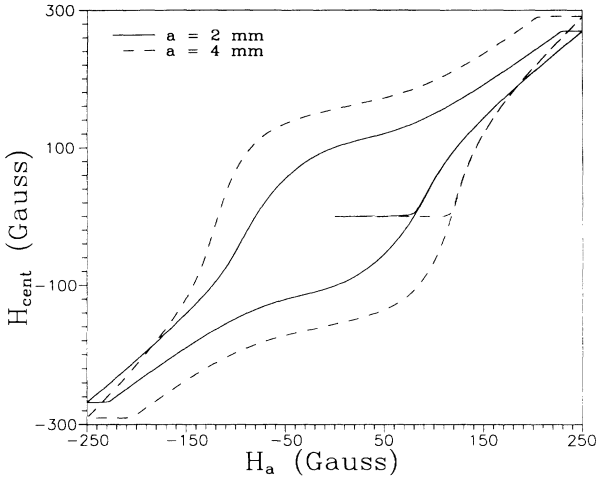

FIG. 6. Experimental example of the demagnetizing effect at $T=35$ K.

$$\frac{\partial H_{\text{cent}}}{\partial H_a}=\left[\frac{\partial H_{\text{cent}}}{\partial H_{\text{eff}}}\right]\left[\frac{\partial H_{\text{eff}}}{\partial H_a}\right]$$
$$=\left[\frac{\partial H_{\text{cent}}}{\partial H_{\text{eff}}}\right]\left[1-N\frac{\partial M}{\partial H_a}\right]. \quad (18)$$

Since $\partial H_{\text{cent}}/\partial H_{\text{eff}}$ is a minimum at $H_{\text{eff}}=0$ ($H_{\text{cent}}=H_p$) and $\partial M/\partial H_a$ has no extrema around $H_a=0$, we conclude that $H_{\text{cent}}=H_p$ when $\partial H_{\text{cent}}/\partial H_a$ is a minimum (and not when $H_a=0$). In Fig. 7 we show this derivative for $a=3$ mm, $L=9$ mm, and $T=50$ K. The noisy features are due to the manner in which $\partial H_{\text{cent}}/\partial H_a$ is calculated (the slope between two adjacent experimental points). This represents a new way of determining H_p and remains valid for the other critical state equations (since they all predict a minimum in $\partial H_{\text{cent}}/\partial H_{\text{eff}}$ at $H_{\text{eff}}=0$).

Using this derivative method, we are able to plot H_p as a function of a [in Figs. 8(a) and 8(b)] for many temperatures ranging from 20 to 85 K. We find that H_p is nonlinear in a. This confirms that J_{cj} is field dependent. An even more pronounced nonlinearity must occur for $a<1$ mm to ensure that $H_p(0)=0$.

We also want to emphasize the fact that we can fit the experimental data even with a demagnetizing effect. This must be done without Eqs. (8) and (9). Instead, Eq. (10) is used since it is still valid in the presence of demagnetizing effects. In Fig. 9(a) and 9(b), the experimental data at 35 and 75 K for $a=4$ mm are fitted using the given values of J_{c0}, H_0, n, N, and f_g. A good agreement is found for the whole temperature and field ranges. The parameters are obtained using an initial H_p representing a compromise between the measured H_p (determined by the derivative method) and the trapped field H_{trapped}. This extra correction is necessary to minimize the impact of end effects,[21] which are discussed in the next paragraph. By fixing n, we vary H_0 in Eq. (10) to obtain different values of J_{c0} and use the mentioned parameters to create the corresponding loop. Since Nf_g is a fixed value as mentioned

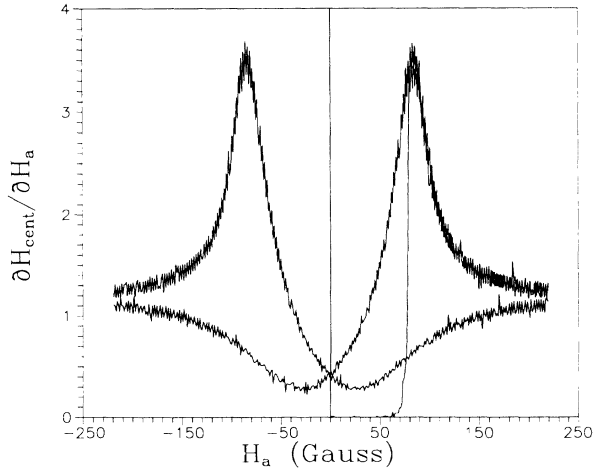

FIG. 7. Derivative of H_{cent} with respect to H_a for $T=50$ K and $a=3$ mm.

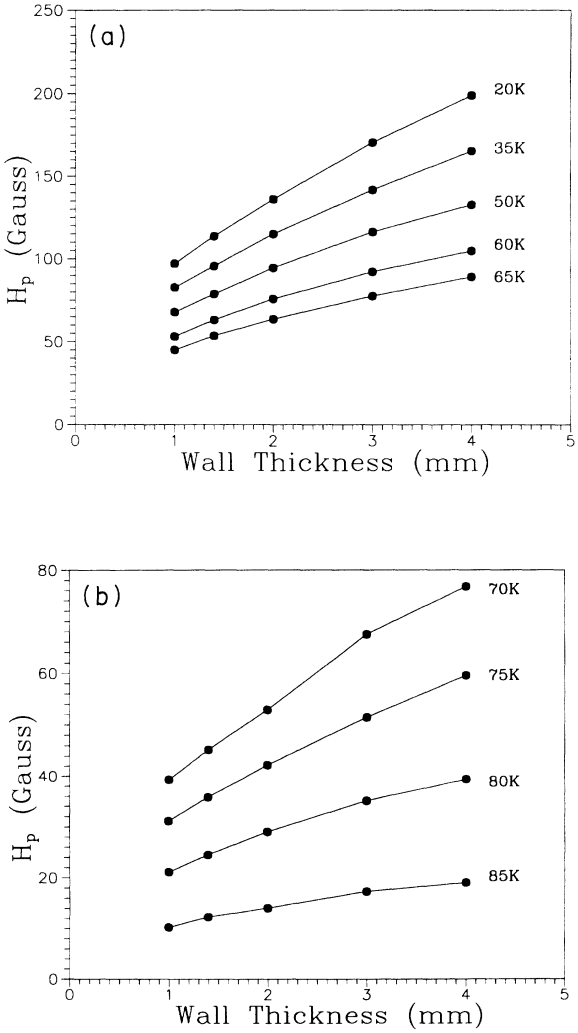

FIG. 8. H_p as a function of the wall thickness for all temperatures.

previously, we also scan individual N and f_g values to obtain the best fit.

We can then use the value of J_{c0}, H_0, and n to fit the wall thickness dependence of H_p. This is shown in Fig. 10 for $T=20$ K. It is seen that the fit follows much more closely the H_p values obtained by the derivative method than those obtained by the trapped field. Furthermore, the increasing difference between H_p and H_{trapped} as one decreases a is a direct evidence of end effects in our low pinning and short length situation. This is confirmed by the difficulty in fitting the entire hysteresis loop for a wall thickness of 1 mm. To take into account this problem, one would have to include a slight axial dependence of the intergrain critical current density which could be similar to a field- (or susceptibility-) dependent demagnetizing factor.[21,22]

In Fig. 11 the H_0 and J_{c0} temperature dependences are presented. J_{c0} has a typical temperature dependence one could expect for the pinning force of a disordered array of Josephson junctions[23] combined with the

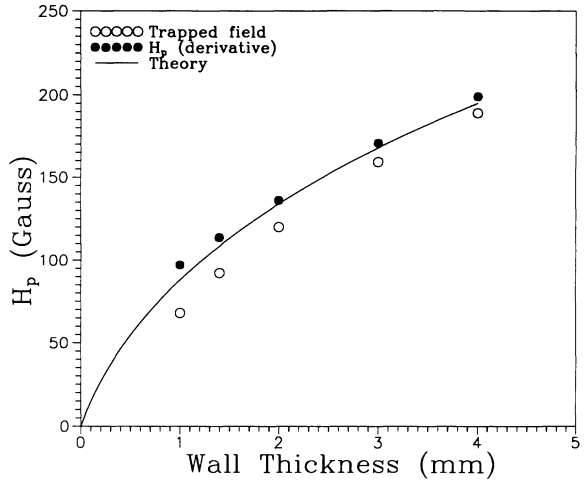

FIG. 10. Comparison of the theoretical value of H_p as a function of the wall thickness with the measured values of H_p (derivative method) and the trapped field ($H_a=0$) at 20 K.

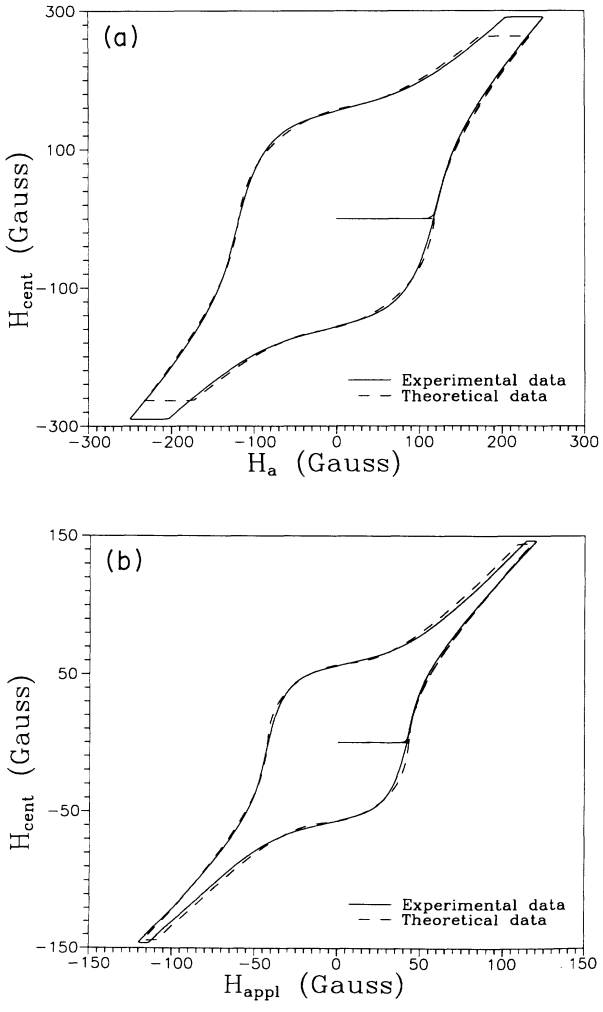

FIG. 9. Experimental data and their corresponding fits: (a) $T=35$ K, $J_{c0}=1250$ A/cm^2, $H_0=90$ G, $n=2$, $f_g=0.54$, and $N=0.40$; (b) $T=75$ K, $J_{c0}=774$ A/cm^2, $H_0=20$ G, $n=2$, $f_g=0.54$, and $N=0.40$.

Ambegaokar-Baratoff[24] expression for the critical current density of a superconductor-insulator-superconductor (SIS) junction (see the detailed discussion on the relation between them in Ref. 18). Thus this parameter can depend on the relative orientation of the grains, particularly because of the great anisotropy (of the gap function) of high-T_c materials. It also depends on the barrier width and the normal resistance of the junctions. These properties can be modified by grain surface contamination, by adding intergrain silver, or by varying the oxygenation.

We also note in Fig. 11 that H_0 presents a positive curvature near T_c, but remains linear below 70 K. The physical significance of H_0 remains unclear. At first instance, one expects H_0 to follow the junction expression given by $\phi_0/r_g\lambda_L$. Contrary to our observations, this gives a negative curvature near T_c proportional to $(1-T/T_c)^{1/2}$. One could argue that H_0 is a measure of the mean distance between pinning centers[25] [$d_0\approx(\phi_0/H_0)^{1/2}$]. This means that H_0 should remain

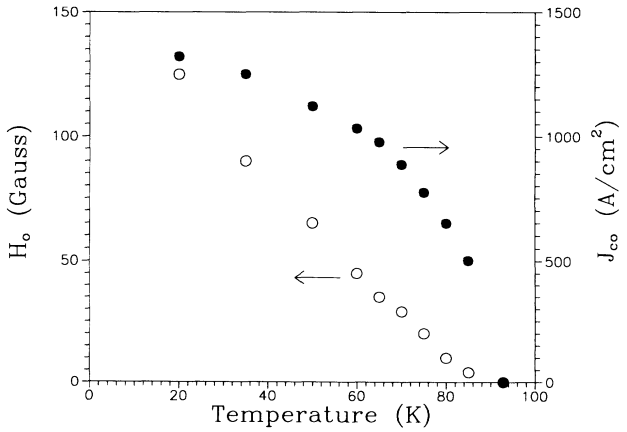

FIG. 11. GCSM parameters J_{c0} and H_0 as a function of temperature deduced from the fits for $a=4$ mm.

constant. Since H_0 varies with temperature as shown in Fig. 11, d_0 is increasing with temperature and diverges at T_c. Our interpretation of H_0 is somewhat different.[26]

Suppose that d_0 is the mean distance between potential pinning sites and d is the mean distance between vortices. If the junction penetration depth λ_J is greater than d_0, a single vortex can include several pinning centers. Thus $d \geq d_0$. Furthermore, we can define H_0 as the local field corresponding to the complete occupancy of the pinning sites. In this condition, the next vortex added to the system at this particular position has no pinning site available and contributes to the decrease of J_c. Since our mean grain radius r_g is around 2.5 μm, we suppose that we always remain in the limit $\lambda_L < r_g$ where λ_L is the mean London penetration depth of the grains. The remainder of this analysis consists in evaluating the effective area covered by one quantum of flux (A_J) excluding the shielded cores of grains. Two limits appear. In the first, λ_J is smaller than r_g. This results in $A_J \approx \lambda_J \lambda_L$ and $H_0 \approx \phi_0/\lambda_J \lambda_L$. The other limit occurs when hypervortices[27] are present giving λ_J greater than r_g. Then one or more grains are embedded in a single vortex. Each grain contributes an area proportional to $r_g \lambda_L$ to the final A_J. The number of grains included in such a vortex is approximately given by λ_J^2/r_g^2 and we obtain $A_J \approx \lambda_J^2 \lambda_L / r_g$ and $H_0 \approx \phi_0 r_g / \lambda_J^2 \lambda_L$. Since λ_J diverges at T_c as $(1-T/T_c)^{-1/2}$, hypervortices will appear near T_c. The extent of this behavior at temperatures lower than T_c will depend on the ratio λ_J/r_g. Using $\lambda_L(T) = 0.74\lambda_L(0)(1-T/T_c)^{-1/2}$, we obtain $H_0(T) \propto (1-T/T_c)^{3/2}$, which reproduces the positive curvature observed in Fig. 11 just below T_c. We note that this theoretical expression gives values of H_0 lower than the experimental H_0 by a factor of 3–5 using realistic values of r_g, λ_L, and λ_J. To explain this difference, we note that the experimental H_0 found with the fit corresponds to a critical current density of $J_{c0}/4$ when $n=2$. Thus our experimental H_0 could be the product of a constant and the above theoretical H_0. Decreasing the temperature at which $\lambda_J \sim r_g$, one should expect a crossover from the hypervortex limit to the junction vortex limit. This qualitative analysis suggests the possibility of varying significantly the transport and magnetic properties by the synthesis of samples with different mean grain radii.[28]

The exponent n is found to remain constant for the whole temperature range at $n=2$. This is consistent with the results presented in Refs. 5 and 29. We expect this exponent to be related to the microstructure of the sample: dimensions and relative orientation of the junctions with respect to the local field. In fact, this value of n is an indication that the mean angle of the junctions with respect to the applied (and local) magnetic field is large.[5,30,31]

We also want to comment on the typical value of $f_g \approx 0.55$ found in this work. The measured density of our sample is 5.23 g/cm^3, which is about 82% of the theoretical density of $YBa_2Cu_3O_7$.[32] If we suppose a radius of 2.5 μm for, say, cylindrical grains[18] penetrated over a London penetration depth of 0.5 μm, we find that the screened volume of the sample is given by $f_g \approx 0.82(1-\lambda_L/r_g)^2$, which is around 50–60 % of the total volume: This is the fitting result. We observe a small temperature dependence of f_g near T_c. It begins to decrease around 80 K, reaching $f_g \approx 0.4$ at 85 K. This is consistent with the fact that λ_L is an increasing function of temperature.

Finally, we have to underline the fact that the three parameters present particular temperature dependences that can be affected during the synthesis. The most interesting avenues are Ag addition,[33–35] texture,[36] and increasing the mean grain radius.[28]

V. CONCLUSION

We underline the importance of understanding the origin of the critical current density limitations from the microstructure of high-T_c polycrystals. In fact, every possible application of these materials in the shape of pellets, bars, or Ag-sheathed tapes will imply a knowledge of the behavior of the parameters of a given critical state equation following precise modifications of the materials.

Here we have used the generalized critical state model (GCSM) to fit entirely the hysteresis loop produced when measuring the field in the center of a YBCO hollow cylinder as a function of the applied field, even in the presence of a demagnetizing effect. The analysis allows one to obtain the model parameters for several temperatures between 20 and 85 K. The full penetration field can be determined using a derivative method, and its corresponding wall thickness dependence can be reproduced theoretically.

ACKNOWLEDGMENTS

The authors wish to thank C. Julien for her technical support throughout the project. We would also like to thank the Natural Sciences and Engineering Research Council (Canada), the Fonds pour la Formation de Chercheurs et l'Aide à la Recherche (Québec), and the Centre de Recherche en Physique du Solide for their financial support.

APPENDIX

In this appendix, we give the analytic solution of the mean field $\langle H(r) \rangle_{\text{inter}}$ which enters in the magnetization calculations. Here the sample is a hollow cylinder of length L, outer radius R, and wall thickness a. The mean field is given by

$$\langle H(r) \rangle_{\text{inter}} = \frac{1}{V} \int_V d^3 r\, H(r) , \tag{A1}$$

where $V = \pi[R^2 - (R-a)^2]L$ is the volume of the sample. Solving Eq. (1) with a surface field of H_{eff} gives the field at position r in the sample as

$$H(r) = [(|H_{\text{eff}}| + H_0)^{n+1} \mp (n+1) J_{c0} H_0^n (R-r)]^{1/(n+1)} - H_0 , \tag{A2}$$

where $-$ and $+$ are for the ascending and descending branches, respectively. Combining Eqs. (A1) and (A2) gives an integral over the radial position, which can be

integrated easily. The result is

$$\langle H(r)\rangle_{\text{inter}}=\Omega\left\{\pm R\Lambda^{n+2/n+1}\mp(R-a)(\Lambda\mp a)^{n+2/n+1}-\frac{n+1}{2n+3}\Lambda^{2n+3/n+1}+\frac{n+1}{2n+3}(\Lambda\mp a)^{2n+3/n+1}\right\}-2H_0\ , \tag{A3}$$

where Ω and Λ are defined as

$$\Omega\equiv\frac{2(n+1)\{(n+1)J_{c0}H_0^n\}^{1/(n+1)}}{R^2-(R-a)^2}\ , \tag{A4}$$

$$\Lambda\equiv\frac{(|H_{\text{eff}}|+H_0)^{n+1}}{(n+1)J_{c0}H_0^n}\ . \tag{A5}$$

In Eq. (A3) the upper sign is for the ascending branch and the lower sign is for the descending one.

One should note that this equation is only valid in the range $H_p\le H_{\text{eff}}\le H_{\text{max}}$ for the ascending branch and $0\le H_{\text{eff}}\le H_{\text{max}}$ for the descending branch. For $0\le H_{\text{eff}}\le H_p$, one has to take into account the sign change in $H(r)$. This gives a similar solution as Eq. (A3) and is not shown here.

[1] J. G. Bednorz and K. A. Müller, Z. Phys. B **64**, 189 (1986).
[2] S. Senoussi, J. Phys. (France) III **2**, 1941 (1992).
[3] J. E. Evetts and B. A. Glowacki, Cryogenics, **28**, 641 (1988).
[4] K.-H. Müller and D. N. Matthews, Physica C **206**, 275 (1993).
[5] K.-H. Müller, D. N. Matthews, and R. Driver, Physica C **191**, 339 (1992).
[6] T. B. Doyle and R. A. Doyle, Cryogenics **32**, 1019 (1992).
[7] P. Fournier and M. Aubin, Cryogenics **33**, 333 (1993).
[8] Y. B. Kim, C. F. Hampstead, and A. R. Strnad, Phys. Rev. **129**, 528 (1963).
[9] E. S. Vlakhov, V. T. Kovachev, M. Polak, and M. Majoros, Physica C **175**, 335 (1991).
[10] M. A.-K. Mohammed and J. Jung, Phys. Rev. B **44**, 4512 (1991).
[11] F. J. Eberhardt, A. D. Hibbs, and A. M. Campbell, Cryogenics **28**, 681 (1988).
[12] S. Senoussi, S. Hadjoudj, C. Weyl, and J. P. Fondere, Physica C **165**, 199 (1990).
[13] H. Castro, E. Holguin, J.-F. Loude, D. Abukay, and L. Rinderer, *Proceedings of the 20th International Conference on Low Temperature Physics, Eugene, Oregon, 1993* [Physica B **194–196**, 1823 (1994)].
[14] P. Fournier and M. Aubin, *Proceedings of the 20th International Conference on Low Temperature Physics* (Ref. 13), p. 1833.
[15] M. Xu., D. Shi, and R. F. Fox, Phys. Rev. B **42**, 10 773 (1990).
[16] S. Senoussi, C. Aguillon, and S. Hadjoudj, Physica C **175**, 215 (1991).
[17] U. Yaron, Y. Kornyushin, and I. Felner, Phys. Rev. B **46**, 14 823 (1992).
[18] J. R. Clem, Physica C **153-155**, 50 (1988).
[19] S. Senoussi, M. Oussena, and S. Hadjoudj, J. Appl. Phys. **63**, 4176 (1988).
[20] R. Laiho, E. Lahderanta, L. Saisa, Gy. Kovacs, G. Zsolt, I. Kirschner, and I. Halasz, Phys. Rev. B **42**, 347 (1990).
[21] A. M. Campbell and J. E. Evetts, Adv. Phys. **21**, 199 (1972). See pp. 272,273.
[22] D. X. Chen, J. A. Brug, and R. B. Goldfarb, IEEE Trans. Magn. **MAG-27**, 3601 (1991).
[23] M. B. Cohn, M. S. Rzchowski, S. P. Benz, and C. J. Lobb, Phys. Rev. B **43**, 12 823 (1991).
[24] V. Ambegaokar and A. Baratoff, Phys. Rev. Lett. **10**, 486 (1963).
[25] P. W. Anderson, Phys. Rev. Lett. **9**, 309 (1962).
[26] J. A. Hulbert, Brit. J. Appl. Phys. **16**, 1657 (1965).
[27] E. B. Sonin and A. K. Tagantsev, Phys. Lett. A **140**, 127 (1989).
[28] L. M. Fisher, V. S. Gorbachev, N. V. Il'in, N. M. Makarov, I. F. Voloshin, V. A. Yampol'skii, R. L. Snyder, S. T. Misture, M. A. Rodriguez, D. P. Matheis, V. R. W. Amarokoon, J. G. Fagun, J. A. T. Taylor, and A. M. M. Barus, Phys. Rev. B **46**, 10 986 (1992).
[29] Q. H. Lam, Y. Kim, and C. D. Jeffries, Phys. Rev. B **42**, 4846 (1990).
[30] A. Barone and G. Paterno, *Physics and Applications of the Josephson Effect* (Wiley, New York, 1982), Chap. 4.
[31] R. L. Peterson and J. W. Ekin, Physica C **157**, 325 (1989).
[32] A. M. T. Bell, Supercond. Sci. Technol. **3**, 55 (1990).
[33] D. Lee and K. Salama, Jpn. J. Appl. Phys. **29**, L2017 (1990).
[34] H. R. Khan, J. R. Thompson, and J. G. Ossandon, Supercond. Sci. Technol. **4**, 133 (1991).
[35] S. Reich and V. M. Nabustovsky, J. Appl. Phys. **68**, 668 (1990).
[36] M. R. Lees, D. Bourgault, D. Braithwaite, P. de Rango, P. Lejay, A. Sulpice, and R. Tournier, Physica C **191**, 414 (1992).